ORIGINAL RESEARCH

A. Tomasian
N. Salamon
M.S. Krishnam
J.P. Finn
J.P. Villablanca

3D High-Spatial-Resolution Cerebral MR Venography at 3T: A Contrast-Dose-Reduction Study

BACKGROUND AND PURPOSE: The effect of various contrast-dose regimens for cerebral MR venography (MRV) has not been previously evaluated at 3T, to our knowledge. Our purpose was to evaluate and compare the diagnostic image quality resulting from half-versus-full-dose contrast regimens for high-spatial-resolution 3D cerebral MRV at 3T.

MATERIALS AND METHODS: Forty consecutive patients with known or suggested cerebrovascular disease underwent 3D high-spatial-resolution ($0.7 \times 0.6 \times 0.9$ mm^3) cerebral contrast-enhanced MRV (CE-MRV) at 3T, by using an identical acquisition protocol. Patients were assigned to 1 of 2 groups: 1) full-dose (~0.1 mmol/kg), and 2) half-dose (~0.05 mmol/kg). Two readers evaluated the resulting images for overall image quality, venous structure definition, and arterial contamination. Signal intensity–to-noise-ratio (SNR) and contrast-to-noise-ratio (CNR) were evaluated in 8 consistent sites. Statistical analysis was performed by using Mann-Whitney U, Wilcoxon signed rank, and t tests and a κ coefficient.

RESULTS: Both readers scored venous-structure definition as excellent or sufficient for diagnosis in approximately 90% of segments for the full-dose group ($\kappa = 0.87$) and in approximately 80% of segments for the half-dose group ($\kappa = 0.85$). Delineation grades were significantly lower for small venous segments, including the middle cerebral, septal, superior cerebellar, inferior vermian, posterior tonsillar, and thalamostriate veins in the half-dose group ($P < .01$). No significant difference existed for arterial contamination grades between the 2 groups ($P > .05$). SNR and CNR values were lower in the half-dose group ($P < .01$).

CONCLUSIONS: At 3T, high-spatial-resolution cerebral MRV can be performed with contrast doses as low as 7.5 mL, without compromising image quality as compared with full-dose protocols, except in the smallest veins, and without compromise of acquisition speed or spatial resolution.

D uring the past decade, flow-sensitive 2D noncontrast time-of-flight and phase-contrast MR venography (MRV) techniques have been used for MRV of intracranial vasculature.[1-6] Recently, contrast-enhanced MRV (CE-MRV), with administration of intravenous gadolinium-based contrast agents (GBCA), has been regarded as an alternative approach,[3,7-14] and promising results have been published using CE-MRV for evaluation of normal dural anatomy, depiction of small-sized intracranial veins and venous structures with low blood flow, and detection of cerebral vaso-occlusive diseases, suggesting the superior image quality of this technique as compared with flow-sensitive 2D MRV.[3,7-9] In addition, parallel imaging techniques make possible increased coverage and sequence performance compared with traditional denser k-space sampling strategies,[15-17] albeit at a cost in signal intensity–to-noise ratio (SNR). This is particularly important for cerebral CE-MRV, in which submillimeter spatial resolution is required for accurate visualization of blood vessels and detection of pathology.[18] The performance of CE-MRV combined with accelerated acquisition for the evaluation of the intracranial venous system has been demonstrated at 1.5T[9] and 3T.[19] The introduction of 3T MR imaging systems to clinical prac-

tice, with higher baseline SNR as compared with 1.5T, has played an important role in the success of highly accelerated parallel acquisition strategies[20] and, when combined with optimized multichannel array coil design, has led to the improved performance of CE-MRV.[19]

Although prior studies have reported successful cerebral CE-MRV with gadolinium doses as low as 0.1–0.15 mmol/kg[7,8] or constant doses corresponding to the same dose range or higher,[3,9,10,12] this generally has involved a compromise in spatial resolution.

In view of the excellent safety record of gadolinium agents and the assumed correlation between image quality and contrast dose, total administered contrast dose has not previously been of great concern. However, recent reports linking GBCA with nephrogenic systemic fibrosis[21-24] have focused attention on the importance of minimizing dose and, by implication, the risk in vulnerable patient subgroups.

Early experience suggests that at 3T, sensitivity to injected paramagnetic contrast agents is heightened for MR angiographic applications.[25-27] However, to our knowledge, the effect of various contrast-dose regimens for cerebral MRV has not been previously evaluated at 3T. We hypothesized that at 3T, relative to full-dose protocols, half-dose contrast protocols would not compromise image quality for cerebral MRV, while improving the cost effectiveness and potentially diminishing the risk of dose-dependent complications. Our purpose was to evaluate and compare the diagnostic image quality resulting from half-versus-full-dose contrast regimens for high-spatial-resolution 3D cerebral MRV at 3T.

BRAIN

ORIGINAL RESEARCH

Materials and Methods

The institutional review board approved our Health Insurance Portability and Accountability Act–compliant study, and the requirement for informed consent was waived because the specific contrast dosage regimens tracked current institutional clinical practice.

Patients

Forty consecutive patients from a single institution, with known or suggested cerebrovascular disease, were evaluated with both 3D high-spatial-resolution CE-MR angiography (CE-MRA) and CE-MRV at 3T. Clinical indications included symptoms of transient ischemic attack ($n = 9$), vertigo/dizziness ($n = 3$), chronic headache ($n = 7$), known or suggested cerebral venous thrombosis ($n = 18$), and intracranial arteriovenous malformation ($n = 3$). Exclusion criteria included all standard contraindications to MR imaging (cardiac pacemaker, claustrophobia, contrast agent allergy, implanted metallic devices). Consecutive patients were sequentially assigned to 1 of 2 groups (A and B), each with 20 patients: group A (12 men, 8 women; mean age, 52.8 years $\pm$ 15.2; age range, 29–81 years) and group B (9 men, 11 women; mean age, 54.5 $\pm$ 17.3 years; age range, 27–79 years). With identical image acquisition protocols, groups A and B received full-dose (15 mL) and half-dose (7.5 mL) gadopentetate dimeglumine (Magnevist; Berlex Laboratories, Wayne, NJ) respectively, during high-spatial-resolution CE-MRA and CE-MRV.

Image Acquisition

All CE-MRA and MRV studies were performed on a 3T whole-body MR imaging system (Magnetom Tim Trio; Siemens Medical Solutions, Erlangen, Germany) equipped with 32 receiver channels and a fast gradient system (peak gradient amplitude, 45 mT/m; slew rate, 200 mT/m/ms). Before examination, a 20-gauge intravenous catheter was placed in an antecubital vein for contrast agent injection. For signal-intensity reception, 22 independent coil elements were used routinely (a 12-channel head matrix coil, a 4-channel neck coil, and a 6-channel spine coil), with coverage extending from the upper thorax to the cranial vertex.

Following 3-plane localizers, a sagittal timing acquisition was performed by using a 3D gradient-recalled echo (GRE) sequence to measure the transit time from the arm vein to the carotid arteries during injection of 1.0-mL Magnevist through an electronic power injector (Spectris Solaris; Medrad, Indianola, Pa) at a rate of 1.2 mL/s. Subsequently, high-spatial-resolution CE-MRA was performed in the coronal plane with a fast spoiled GRE sequence.

Immediately afterward, CE-MRV was performed in a sagittal plane by using a fast GRE sequence (TR/TE, 3.4/1.3 msec; flip angle, 25°; bandwidth, 610 Hz/pixel) with elliptic centric k-space. In an elliptic centric phase-encoding acquisition, the low-spatial-frequency k-space data (center of k-space) are acquired at the beginning of the imaging period. This enhances the flexibility of the protocol to synchronize imaging to coincide with maximal venous enhancement. A generalized autocalibrating partially parallel acquisition[17] factor of 6 (phase-encoding direction $\times$ 3, section-encoding direction $\times$ 2) was implemented with 24 reference k-space lines for calibration in each direction. These settings allowed acquisition of 160 partitions over a 300×244 mm FOV with the k-space matrix of 374×512 and resultant true voxel dimensions of $0.7 \times 0.6 \times 0.9$ mm^3 in 24 seconds. An asymmetric k-space sampling scheme (partial Fourier 75%) was applied in all 3 planes to minimize the TE and the acquisition time. CE-MRV protocol was a non-breath-hold acquisition.

Incrementally, we decreased the dosage of contrast agent (Magne-

vist Solution) from 15 to 7.5 mL gadolinium. At both dose levels, the infusion period was fixed at 15 seconds, corresponding to 1 mL/s and 0.5 mL/s, respectively. For groups A and B, the contrast was diluted with normal saline by a factor of 2 and 3, respectively, to maintain equivalent injected volumes and rates. Patients were sequentially included in 2 groups, on the basis of the following dosage regimens:

1) Group A (full dose): 15 mL, corresponding to 0.104 $\pm$ 0.012 mmol/kg body weight.

2) Group B (half dose): 7.5 mL, corresponding to 0.051 $\pm$ 0.008 mmol/kg body weight.

After data acquisition, image processing was performed on a separate 3D workstation (Leonardo; Siemens), with standard commercial software by using a maximum intensity projection (MIP) algorithm. The entire 3D volume was reconstructed in overlapping thin MIP subvolumes (10-mm thick, overlapped by 9 mm) in coronal, sagittal, and axial planes. In addition, full-volume MIP and 3D volume-rendered images in a 360° rotation range were generated at the same workstation. All of the reconstructed data, as well as the source images, were available to both readers for analysis.

Image Analysis

The MR imaging datasets from both groups were presented in a blinded random fashion to 2 board-certified neuroradiologists with at least 5 years of experience. The images were evaluated independently and during separate reading sessions. Both readers were blinded to the patients' identities, clinical information, and contrast agent–dose protocol. The readers were instructed to use both the source images and the postprocessed data available on a workstation for analysis.

The readers evaluated the overall quality of MRVs with regard to venous enhancement, and presence of artifacts (including parallel acquisition reconstruction artifact, motion artifact, and/or noise) by using a scoring scale of 1–3: grade 1, poor image quality, inadequate venous enhancement and/or the presence of a significant amount of artifacts/noise impairing the diagnosis; grade 2, good image quality sufficient for diagnosis, adequate venous enhancement, and/or mild-to-moderate amounts of artifacts/noise not interfering with diagnosis; grade 3, excellent image quality for highly confident diagnosis, good venous enhancement, and no-to-minimal amount of artifacts/noise.

The intra- and extracranial venous structures, including cerebral venous sinuses and major superficial and deep cerebral veins, were divided into 32 segments (Table 1). The continuity, visibility, and edge sharpness of the intracranial venous segments were assessed in each patient. Visualization of venous structures was assessed by using a scoring scale of 1–4: grade 1, not visible; grade 2, partially visible, not sufficient for diagnosis; grade 3, generally homogeneous enhancement and continuity of venous structure, sufficient for diagnosis; and grade 4, excellent image quality with highly homogeneous and continuous enhancement and conspicuous sharpness of vessel border, allowing highly confident diagnosis. The image quality of a venous segment was rated as diagnostic (grade, $\geq$3) if the reader was confidently able to visualize the lumen of the venous structure in its entirety, whether it was clearly normal, pathologically thrombosed or invaded, or hypoplastic.

Potentially contaminating arterial enhancement was evaluated on a scale of 0–3: grade 0, none; grade 1, minimal, allowing interpretation with a high degree of diagnostic confidence; grade 2, moderate, exceeding acceptable degree and limiting diagnostic confidence; and grade 3, severe, markedly limiting diagnostic confidence.

Table 1: Visualization of venous segments on full-dose and half-dose high-spatial-resolution CE-MRV ($n = 640$)*

| Location | Reader 1 | | | Reader 2 | | |
| | Full-Dose (half-dose) CE-MRV | | | Full-Dose (half-dose) CE-MRV | | |
	Mean ± SD	Median	Range	Mean ± SD	Median	Range
Superior sagittal sinus	4.00 ± 0.00 (4.00 ± 0.00)	4 (4)	4–4 (4–4)	4.00 ± 0.00 (4.00 ± 0.00)	4 (4)	4–4 (4–4)
Inferior sagittal sinus	3.45 ± 0.60 (3.40 ± 0.68)	3.5 (3.5)	2–4 (2–4)	3.55 ± 0.60 (3.45 ± 0.69)	4 (4)	2–4 (2–4)
Transverse sinus	3.97 ± 0.16 (4.00 ± 0.00)	4 (4)	3–4 (4–4)	4.00 ± 0.00 (4.00 ± 0.00)	4 (4)	4–4 (4–4)
Sigmoid sinus	3.97 ± 0.16 (3.97 ± 0.16)	4 (4)	3–4 (3–4)	4.00 ± 0.00 (4.00 ± 0.00)	4 (4)	4–4 (4–4)
Straight sinus	3.95 ± 0.22 (3.90 ± 0.31)	4 (4)	3–4 (3–4)	3.90 ± 0.31 (3.95 ± 0.22)	4 (4)	3–4 (3–4)
Cavernous sinus	3.72 ± 0.60 (3.70 ± 0.52)	4 (4)	2–4 (2–4)	3.70 ± 0.65 (3.62 ± 0.59)	4 (4)	2–4 (2–4)
Superior petrosal sinus	3.05 ± 0.75 (2.97 ± 0.66)	3 (3)	1–4 (1–4)	2.95 ± 0.71 (2.90 ± 0.67)	3 (3)	1–4 (1–4)
Torcula herophili	4.00 ± 0.00 (4.00 ± 0.00)	4 (4)	4–4 (4–4)	4.00 ± 0.00 (4.00 ± 0.00)	4 (4)	4–4 (4–4)
Cortical vein	3.97 ± 0.16 (3.97 ± 0.16)	4 (4)	3–4 (3–4)	3.92 ± 0.27 (3.95 ± 0.22)	4 (4)	3–4 (3–4)
Vein of Galen	3.95 ± 0.22 (3.90 ± 0.31)	4 (4)	3–4 (3–4)	3.90 ± 0.31 (3.85 ± 0.37)	4 (4)	3–4 (3–4)
Internal cerebral vein	3.65 ± 0.53 (3.55 ± 0.64)	4 (4)	2–4 (2–4)	3.62 ± 0.54 (3.52 ± 0.64)	4 (4)	2–4 (2–4)
Middle cerebral vein	3.25 ± 0.67 (2.37 ± 0.87)	3 (2)	2–4 (1–4)	3.25 ± 0.71 (2.37 ± 0.84)	3 (2.5)	2–4 (1–4)
Basal vein of Rosenthal	3.40 ± 0.68 (3.20 ± 0.70)	3.5 (3)	2–4 (2–4)	3.35 ± 0.75 (3.35 ± 0.67)	3.5 (3)	2–4 (2–4)
Septal vein	2.95 ± 0.60 (2.35 ± 0.81)	3 (2)	2–4 (1–4)	2.95 ± 0.69 (2.35 ± 0.75)	3 (2.5)	2–4 (1–3)
Superior cerebellar vein	2.72 ± 0.60 (2.32 ± 0.76)	3 (2.5)	1–4 (1–3)	2.82 ± 0.68 (2.37 ± 0.77)	3 (3)	1–4 (1–4)
Posterior tonsillar vein	2.87 ± 0.56 (2.37 ± 0.63)	3 (2)	2–4 (1–3)	3.00 ± 0.60 (2.45 ± 0.68)	3 (2.5)	2–4 (1–4)
Inferior vermian vein	2.70 ± 0.73 (2.15 ± 0.74)	3 (2)	2–4 (1–3)	2.85 ± 0.75 (2.25 ± 0.79)	3 (2)	2–4 (1–3)
Superior ophthalmic vein	3.62 ± 0.59 (3.55 ± 0.60)	4 (4)	2–4 (2–4)	3.70 ± 0.52 (3.55 ± 0.55)	4 (4)	2–4 (2–4)
Thalamostriate vein	2.67 ± 0.73 (2.25 ± 0.74)	3 (2)	1–4 (1–3)	2.62 ± 0.74 (2.22 ± 0.73)	3 (2)	1–4 (1–3)
Internal jugular vein	4.00 ± 0.00 (4.00 ± 0.00)	4 (4)	4–4 (4–4)	4.00 ± 0.00 (4.00 ± 0.00)	4 (4)	4–4 (4–4)

Note:—CE-MRV indicates contrast-enhanced MR venography.
* The 4-point scale for evaluation of visualization of venous segments is as follows: grade 1, not visible; grade 2, partially visible, not sufficient for diagnosis; grade 3, generally homogeneous enhancement and continuity of venous structure, sufficient for diagnosis; and grade 4, excellent image quality with highly homogeneous and continuous enhancement with sharpness of vessel border allowing highly confident diagnosis. There was no significant difference in the vessel delineation scores assigned by the 2 readers ($P > .05$ for all segments). Analysis with the κ coefficient revealed excellent interobserver agreement for the full-dose ($\kappa = 0.87$) and half-dose ($\kappa = 0.85$) groups. Delineation scores were significantly lower for the small venous segments, including the middle cerebral, septal, superior cerebellar, inferior vermian, posterior tonsillar, and thalamostriate veins in the half-dose group compared with the single-dose group ($P < .01$ for all).

SNR and contrast-to-noise ratio (CNR) were measured for the following venous segments: the superior sagittal sinus, inferior sagittal sinus, straight sinus, transverse sinus, sigmoid sinus, vein of Galen, internal cerebral vein, and internal jugular vein for both contrast-dose groups. SNR was calculated as the signal intensity (SI) from the desired venous segment divided by SD of the background noise, which was determined by an average value from 6 extracorporal regions. CNR was calculated by determining the difference in SI between the desired venous segment and the adjacent tissue divided by the SD of the background noise.

Statistical Analysis

The Mann-Whitney *U* test and the Wilcoxon signed rank test were used to evaluate the significance of the differences in overall image quality, venous visibility and sharpness, and arterial contamination scores between the 2 groups for each reader and between the readers, respectively. The SNR and CNR values for the 2 groups were analyzed by the Student *t* test. Interobserver agreement for the scores assigned for assessment of overall image quality and visibility and sharpness of venous segments between the 2 readers was determined by calculating the κ coefficient (poor agreement, $\kappa = 0$; slight agreement, $\kappa = 0.01$–0.2; fair agreement, $\kappa = 0.21$–0.4; moderate agreement, $\kappa = 0.41$–0.6; good agreement, $\kappa = 0.61$–0.8; and excellent agreement, $\kappa = 0.81$–1). For all statistical tests, a 2-sided $P < .05$ was used as the criterion of significance.

Results

All examinations were completed successfully, and all contrast agent administrations were performed without complications.

Overall Image Quality

Reader 1 graded the overall image quality as excellent in 18 and good in 2 patients in the full-dose group. Reader 2 graded the overall image quality as excellent in 19 and good in 1 patient in the full-dose group (median, 3; range, 2–3) ($\kappa = 0.64$; 95% confidence interval [CI], 0.58–0.70). In the half-dose group, reader 1 graded the overall image quality as excellent in 16 and good in 4 patients. In the half-dose group, reader 2 graded the overall image quality as excellent in 18 and good in 2 patients (median, 3; range, 2–3) ($\kappa = 0.62$; 95% CI, 0.57–0.67). There was no significant difference for overall image quality scores between the 2 dose groups for each reader ($P > .05$) or between the readers ($P > .05$) (Fig 1). Parallel acquisition reconstruction artifacts were not noted, and image noise was not found to interfere with diagnostic image quality in any case.

Evaluation of Venous Structure Definition on Full- and Half-Dose CE-MRV

In the full-dose group, of 640 venous segments for possible evaluation, 98.8% (632/640) of segments were visualized by both readers. Reader 1 identified 90.3% (578/640) of segments with grades for definition in the diagnostic range (grades 3 and 4) and 9.7% (62/640) of segments with insufficient definition for diagnosis (grades 1 and 2). Reader 2 identified 90% (580/640) of segments with grades for definition in the diagnostic range (grades 3 and 4) and 10% (64/640) of segments with insufficient definition for diagnosis (grades 1 and 2). There was no statistically significant difference in venous visibility and sharpness grades assigned by the 2 readers ($P > .05$ for all segments). The overall interobserver agreement for the as-
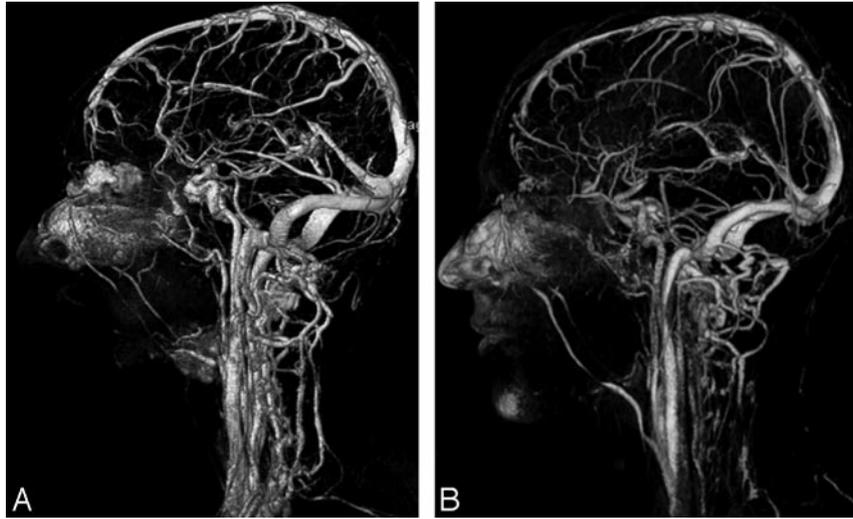
Fig 1. 3D volume-rendered images from full-dose (15 mL) (*A*) and half-dose (7.5 mL) (*B*) contrast-enhanced MRV show diagnostic image quality of most of the cerebral venous structures.
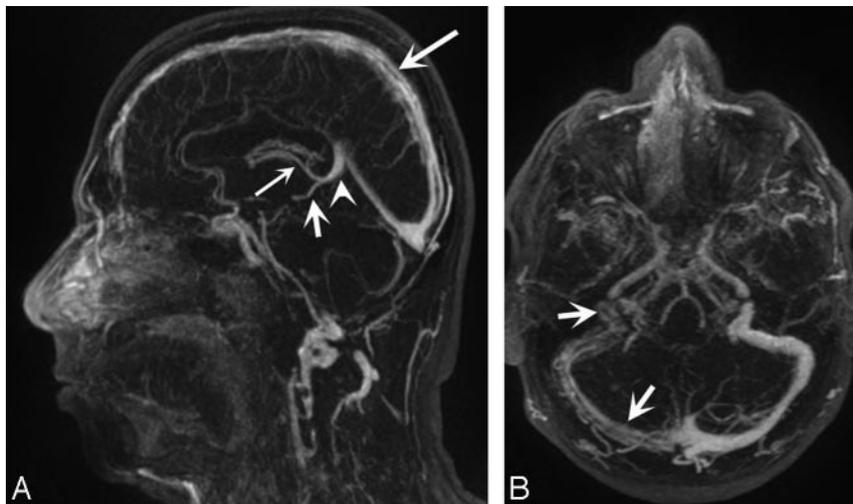

Fig 2. Half-dose CE-MRV. Sagittal (*A*) and axial (*B*) thin MIP images (TR/TE, 3.4/1.3 ms; flip angle, 25°) in a 28-year-old man with history of headache show filling defects within the superior sagittal sinus (*A, large arrow*) and transverse and sigmoid sinuses (*B, small arrows*) consistent with thrombosis. Note the high diagnostic quality of the vein of Galen (*A, arrowhead*), the basal vein of Rosenthal (*A, small arrow*), and the internal cerebral veins (*A, thin large arrow*).

signed delineation grades was excellent (κ = 0.87; 95% CI, 0.83–0.91).

In the half-dose group (Figs 2 and 3), of 640 venous segments for possible evaluation, 95% (608/640) of segments were visualized by both readers. Reader 1 identified 80% (512/640) of segments with grades for definition in the diagnostic range (grades 3 and 4) and 20% (128/640) of segments with insufficient definition for diagnosis (grades 1 and 2). Reader 2 identified 80.9% (518/640) of segments with grades for definition in the diagnostic range (grades 3 and 4) and 19.1% (122/640) of segments with insufficient definition for diagnosis (grades 1 and 2). There was no statistically significant interreader difference in venous visibility and sharpness grades assigned (P > .05 for all segments). The overall interobserver agreement for the assigned delineation grades was excellent (κ = 0.85; 95% CI, 0.81–0.89).

Comparison of venous delineation grades assigned by each reader between the 2 groups by using the Mann-Whitney U test demonstrated significantly lower grades for small venous segments, including the middle cerebral, septal, superior cer-

ebellar, inferior vermian, posterior tonsillar, and thalamostriate veins in the half-dose group as compared with the single-dose group (P < .01 for all). No statistically significant difference existed for the delineation grades assigned to the other venous segments (P > .05 for all) (Table 1).

Evaluation of Contaminating Arterial Enhancement on Full- and Half-Dose CE-MRV

For visualized segments, in the full-dose group, reader 1 graded contaminating arterial enhancement as none in 98.6% (623/632), minimal in 1.1% (7/632) (cavernous sinus, n = 7), and moderate in 0.3% (2/632) (cavernous sinus, n = 2) of venous segments. Likewise, reader 2 graded contaminating arterial enhancement as none in 98.4% (622/632), minimal in 1.3% (8/632) (cavernous sinus, n = 8), and moderate in 0.3% (2/632) (cavernous sinus, n = 2) of venous segments.

For the half-dose group, reader 1 graded contaminating arterial enhancement as none in 98.7% (600/608), minimal in 1.1% (7/608) (cavernous sinus, n = 7), and moderate in 0.2% (1/608) (cavernous sinus, n = 2) of venous segments. Like-
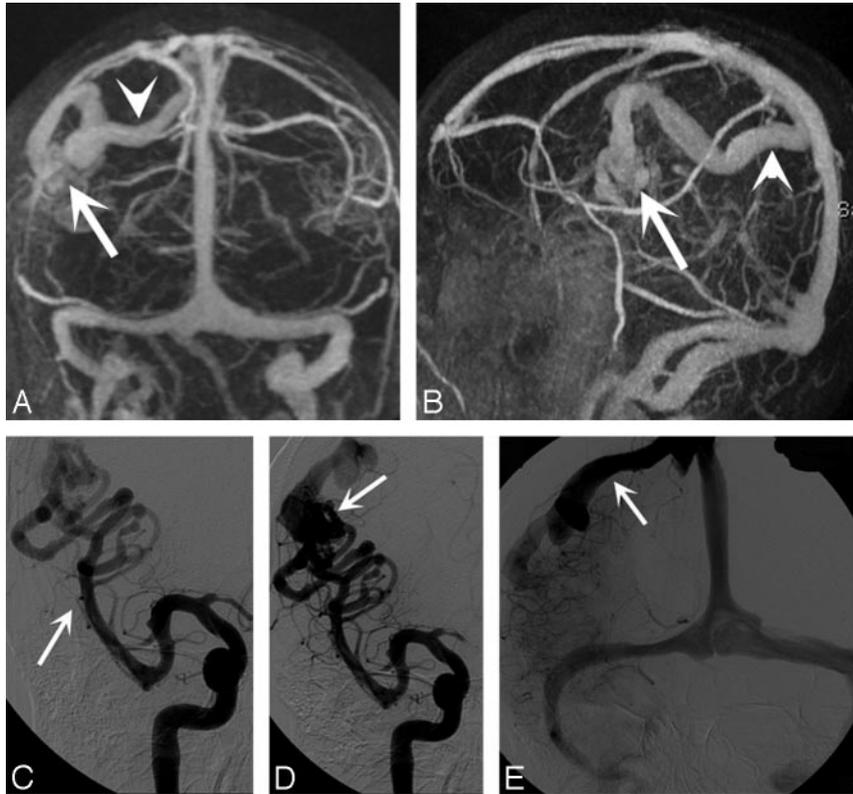
Fig 3. Half-dose CE-MRV. *A* and *B*, Coronal (*A*) and sagittal (*B*) full-thickness MIP images (TR/TE, 3.4/1.3 ms; flip angle, 25°) in a 27-year-old man show cerebral arteriovenous malformation nidus (*A* and *B*, *arrow*) and a large draining vein to the superior sagittal sinus (*A* and *B*, *arrowhead*). *C–E*, DSAs confirm the findings on CE-MRV. Feeder artery (middle cerebral artery) (*C*, *arrow*), arteriovenous malformation nidus (*D*, *arrow*), and draining vein to the superior sagittal sinus (*E*, *arrow*) are clearly visualized.

Table 2: SNR and CNR in full- and half-dose CE-MRV*

	Full-Dose CE-MRV		Half-Dose CE-MRV	
	SNR	CNR	SNR	CNR
Superior sagittal sinus	611.5 ± 82.3	501.3 ± 77.6	322.2 ± 45.1	291.3 ± 41.6
Inferior sagittal sinus	276.8 ± 31.2	236.5 ± 29.3	158.7 ± 23.3	132.7 ± 21.5
Straight sinus	508.8 ± 77.6	461.1 ± 70.9	234.5 ± 32.6	203.8 ± 28.8
Transverse sinus	532.9 ± 81.2	479.2 ± 75.4	302.2 ± 45.6	269.3 ± 40.9
Sigmoid sinus	555.4 ± 84.6	497.6 ± 79.4	309.4 ± 48.1	261.8 ± 43.3
Vein of Galen	490.7 ± 62.3	434.2 ± 58.2	224.4 ± 29.7	194.4 ± 26.9
Internal cerebral vein	390.1 ± 58.8	342.1 ± 50.8	201.3 ± 31.3	168.6 ± 30.2
Internal jugular vein	572.6 ± 81.1	516.6 ± 72.9	334.8 ± 44.5	305.8 ± 40.8

Note:—SNR indicates signal intensity-to-noise ratio; CNR, contrast-to-noise ratio.

* All values are presented as mean ± SD. SNR and CNR values are significantly lower in the half-dose CE-MRV group compared with the single-dose CE-MRV group ($P < .001$ for all segments).

wise, reader 2 graded contaminating arterial enhancement as none in 99% (602/608), minimal in 0.8% (5/608) (cavernous sinus, $n = 5$), and moderate in 0.2% (1/608) (cavernous sinus, $n = 2$) of venous segments.

No statistically significant difference existed in arterial contamination grades assigned by each reader between the 2 groups ($P > .05$ for both readers).

Details of SNR and CNR values for venous segments are given in Table 2. Statistical analysis revealed significantly lower SNR ($P < .01$) and CNR ($P < .01$) values for evaluated venous segments in the half-dose group compared with the full-dose group. However, these differences on the images were not subjectively apparent to the reviewers.

Additional findings on the full-dose CE-MRV included arachnoid granulation (superior sagittal sinus, $n = 3$; transverse sinus, $n = 2$; sigmoid sinus, $n = 2$), transverse sinus

thrombosis ($n = 6$), hypoplastic transverse sinus ($n = 3$), and arteriovenous malformation ($n = 1$). In the half-dose group, findings included arachnoid granulation (superior sagittal sinus, $n = 4$; transverse sinus, $n = 2$; sigmoid sinus, $n = 2$), hypoplastic transverse sinus ($n = 1$), transverse sinus thrombosis ($n = 7$), superior sagittal sinus occlusion ($n = 1$), and arteriovenous malformation ($n = 2$). The findings were confidently evaluated by both readers.

Discussion

The results of our study indicate that at 3T, high-spatial-resolution cerebral CE-MRV can be performed with a fraction of the contrast dose commonly used in routine practice, without compromise in pulse sequence performance or image quality for evaluation of major extra- and intracranial venous structures. We did observe that the visibility and sharpness of very

small intracranial venous segments were significantly lower in the half-dose CE-MRV group compared with the full-dose group. Because very small veins are uncommonly involved in symptomatic disease in the absence of concomitant larger dural sinus involvement, we believe this difference is not likely to be relevant in routine clinical practice.

Cerebral CE-MRV at 3T has emerged as a powerful noninvasive diagnostic tool for evaluation of intracranial venous structures.[19] However, in the past there has been little emphasis on gadolinium contrast-dose minimization strategies. In this context, we sought to determine whether preservation of image quality could be achieved by decreasing the contrast dose without significantly sacrificing image quality.

At 3T, sequence performance is generally higher compared with lower field strength due to the higher available baseline SNR, which is used to increase speed, coverage, and /or spatial resolution by the use of parallel acquisition schemes. Because SNR is inversely related to spatial resolution, 1 approach to compensate for decreased contrast dose is to compromise on spatial resolution. However, for confident assessment of intracranial venous systems, a premium is placed on image quality and spatial resolution.[19]

Successful application of CE-MR protocols with sufficient spatial resolution is related to the vascular SNR. Besides magnetic field strength and contrast agent relaxivity, SNR is directly proportional to the square root of TR/T1 and is inversely related to the square root of the acceleration factor and the coil geometry factor.

We agree with others that by raising the baseline signal intensity with stronger magnetic fields,[25,26] using contrast agents with high relaxivity,[28,29] reducing noise amplification by using receiver coils with more channels, and achieving optimized geometry and high-sensitivity profiles,[30,31] the SNR level can be preserved. In addition, parallel acquisition–associated SNR penalty is mitigated at 3T.[32,33]

In our study, the measured SNR and CNR values in the evaluated venous segments were significantly lower with the half-dose protocol compared with the full-dose protocol. However, the SNR and CNR were still adequate for confident evaluation of these segments, and there was no significant difference in the delineation grades of most venous segments between the 2 groups. Nevertheless, the visibility and sharpness of very small intracranial venous segments, including the middle cerebral, septal, superior cerebellar, inferior vermian, posterior tonsillar, and thalamostriate veins were significantly lower with the half-dose protocol. This may be attributed to the fact that sufficient SNR and CNR values were not achieved for these segments. Our results suggest that with our specific commercially available hardware configuration, there is little advantage to using higher contrast-dose protocols for assessment of major intracranial venous structures, which are the chief focus of clinically important questions. It is the high spatial resolution of the CE-MRV technique that is critical for visualization of venous segments and detection of venous abnormalities

Previous studies have successfully implemented CE-MRV protocols for imaging of intracranial venous structures with the use of a single dose or higher doses of GBCA.[3,7-9,19]

Farb et al[3] implemented a 3D GRE sequence with elliptic centric ordering achieving voxel dimensions of $0.78 \times 0.78 \times$

1.3 mm³ at 1.5T. The investigators injected a fixed dose of 30 mL of contrast medium, and complete visibility was gained for 92% of segments.

Hu et al[9] performed cerebral MRV at 1.5T, with a fourfold acceleration using a fast spoiled GRE sequence generating voxel dimensions of $0.8 \times 0.8 \times 1.4$ mm³ in 65 seconds while injecting a fixed dose of 19 mL. Excellent overall diagnostic image quality was gained in 80% of patients. Nael et al[19] implemented a 3D fast GRE sequence at 3T with an acceleration factor of 6 during injection of 0.15 mmol/kg of contrast agent (voxel dimensions $0.7 \times 0.7 \times 0.8$ mm³), and diagnostic image quality was achieved in 90% of cerebral venous segments.

Our study at 3T indicates that despite using a fast high-spatial-resolution acquisition, image quality is comparable between full-dose and half-dose gadolinium infusion protocols for major intracranial venous segments.

Our study has some limitations. The 2 contrast agent–dose protocols evaluated were not applied to each individual. Therefore, comparison of the intraindividual diagnostic image quality was not possible. Second, we did not undertake a comparison of the diagnostic sensitivity and specificity of this technique because doing so would require comparison with the gold standard, digital subtraction angiography (DSA), which was not realistic in such a large patient cohort. We believe further studies are warranted for additional assessment of diagnostic sensitivity and specificity of half-dose CE-MRV in correlation with DSA. Moreover, many of the patients in our study had no or low suggestion of cerebral venous disease. However, because the purpose of the study was to show the technical feasibility of the described half-dose protocol, the significance of this limitation was mitigated. Some of the venous structures, which were not visualized in this study, were possibly absent (normal variation), thus artifactually decreasing our venous structure visualization rates. However, this could not be verified due to the lack of a gold standard.

Conclusions
Our study shows that by exploiting the higher SNR available at 3T in combination with multichannel coils and by effectively using highly accelerated parallel imaging, high-spatial-resolution cerebral CE-MRV at 3T can be performed with a gadolinium dose as low as 7.5 mL, without compromising image quality as compared with the full-dose protocol (15 mL). The clinical accuracy of this technique needs to be investigated in a broader clinical setting in a population of patients with cerebral venous disease.

References
1. Mattle HP, Wentz KU, Edelman RR, et al. **Cerebral venography with MR.** *Radiology* 1991;178:453–58
2. Liauw L, van Buchem MA, Spilt A, et al. **MR angiography of the intracranial venous system.** *Radiology* 2000;214:678–82
3. Farb RI, Scott JN, Willinsky RA, et al. **Intracranial venous system: gadolinium-enhanced three-dimensional MR venography with auto-triggered elliptic centric-ordered sequence—initial experience.** *Radiology* 2003;226:203–09
4. Ayanzen RH, Bird CR, Keller PJ, et al. **Cerebral MR venography: normal anatomy and potential diagnostic pitfalls.** *AJNR Am J Neuroradiol* 2000;21:74–78
5. Pui MH. **Cerebral MR venography.** *Clin Imaging* 2004;28:85–89
6. Fera F, Bono F, Messina D, et al. **Comparison of different MR venography techniques for detecting transverse sinus stenosis in idiopathic intracranial hypertension.** *J Neurol* 2005;252:1021–25
7. Liang L, Korogi Y, Sugahara T, et al. **Normal structures in the intracranial dural sinuses: delineation with 3D contrast-enhanced magnetization pre-**

pared rapid acquisition gradient-echo imaging sequence. *AJNR Am J Neuroradiol* 2002;23:1739–46

8. Rollins N, Ison C, Reyes T, et al. **Cerebral MR venography in children: comparison of 2D time-of-flight and gadolinium-enhanced 3D gradient-echo techniques.** *Radiology* 2005;235:1011–17

9. Hu HH, Campeau NG, Huston J, et al. **High-spatial-resolution contrast-enhanced MR angiography of the intracranial venous system with fourfold accelerated two-dimensional sensitivity encoding.** *Radiology* 2007;243:853–61

10. Lovblad KO, Schneider J, Bassetti C, et al. **Fast contrast-enhanced MR whole-brain venography.** *Neuroradiology* 2002;44:681–88

11. Kirchhof K, Welzel T, Jansen O, et al. **More reliable noninvasive visualization of the cerebral veins and dural sinuses: comparison of three MR angiographic techniques.** *Radiology* 2002;224:804–10

12. Wetzel SG, Law M, Lee VS, et al. **Imaging of the intracranial venous system with a contrast-enhanced volumetric interpolated examination.** *Eur Radiol* 2003;13:1010–18

13. Lee JM, Jung S, Moon KS, et al. **Preoperative evaluation of venous systems with 3-dimensional contrast-enhanced magnetic resonance venography in brain tumors: comparison with time-of-flight magnetic resonance venography and digital subtraction angiography.** *Surg Neurol* 2005;64:128–33

14. Mermuys KP, Vanhoenacker PK, Chappel P, et al. **Three-dimensional venography of the brain with a volumetric interpolated sequence.** *Radiology* 2005;234:901–08

15. Sodickson DK, McKenzie CA, Li W, et al. **Contrast-enhanced 3D MR angiography with simultaneous acquisition of spatial harmonics: a pilot study.** *Radiology* 2000;217:284–89

16. Pruessmann KP, Weiger M, Scheidegger MB, et al. **SENSE: sensitivity encoding for fast MRI.** *Magn Reson Med* 1999;42:952–62

17. Griswold MA, Jakob PM, Heidemann RM, et al. **Generalized autocalibrating partially parallel acquisitions (GRAPPA).** *Magn Reson Med* 2002;47:1202–10

18. Leclerc X, Nicol L, Gauvrit JY, et al. **Contrast-enhanced MR angiography of supraaortic vessels: the effect of voxel size on image quality.** *AJNR Am J Neuroradiol* 2000;21:1021–27

19. Nael K, Fenchel M, Salamon N, et al. **Three-dimensional cerebral contrast-enhanced magnetic resonance venography at 3.0 Tesla: initial results using highly accelerated parallel acquisition.** *Invest Radiol* 2006;41:763–68

20. Pruessmann KP. **Parallel imaging at high field strength: synergies and joint potential.** *Top Magn Reson Imaging* 2004;15:237–44

21. Hedley AJ, Molan MP, Hare DL, et al. **Nephrogenic systemic fibrosis associated with gadolinium-containing contrast media administration in patients with reduced glomerular filtration rate.** *Nephrology (Carlton)* 2007;12:111

22. Sadowski EA, Bennett LK, Chan MR, et al. **Nephrogenic systemic fibrosis: risk factors and incidence estimation.** *Radiology* 2007;243:148–57. Epub 2007 Jan 31

23. Perazella MA, Rodby RA. **Gadolinium-induced nephrogenic systemic fibrosis in patients with kidney disease.** *Am J Med* 2007;120:561–62

24. Thomsen HS, Morcos SK. **Nephrogenic systemic fibrosis and nonionic linear chelates.** *AJR Am J Roentgenol* 2007;188:W580, author reply W581

25. Campeau NG, Huston J 3rd, Bernstein MA, et al. **Magnetic resonance angiography at 3.0 Tesla: initial clinical experience.** *Top Magn Reson Imaging* 2001;12:183–204

26. Willinek WA, Born M, Simon B, et al. **Time-of-flight MR angiography: comparison of 3.0-T imaging and 1.5-T imaging—initial experience.** *Radiology* 2003;229:913–20

27. Rinck PA, Muller RN. **Field strength and dose dependence of contrast enhancement by gadolinium-based MR contrast agents.** *Eur Radiol* 1999;9:998–1004

28. Fink C, Puderbach M, Ley S, et al. **Contrast-enhanced three-dimensional pulmonary perfusion magnetic resonance imaging: intraindividual comparison of 1.0 M gadobutrol and 0.5 M Gd-DTPA at three dose levels.** *Invest Radiol* 2004;39:143–48

29. Nael K, Fenchel M, Krishnam M, et al. **3.0 Tesla high spatial resolution contrast-enhanced magnetic resonance angiography (CE-MRA) of the pulmonary circulation: initial experience with a 32-channel phased array coil using a high relaxivity contrast agent.** *Invest Radiol* 2007;42:392–98

30. Weiger M, Pruessmann KP, Leussler C, et al. **Specific coil design for SENSE: a six-element cardiac array.** *Magn Reson Med* 2001;45:495–504

31. de Zwart JA, Ledden PJ, van Gelderen P, et al. **Signal-to-noise ratio and parallel imaging performance of a 16-channel receive-only brain coil array at 3.0 Tesla.** *Magn Reson Med* 2004;51:22–26

32. Nael K, Villablanca JP, McNamara TO, et al. **Supraaortic arteries: contrast-enhanced MR angiography at 3.0 T—highly accelerated parallel acquisition for improved spatial resolution over an extended field of view.** *Radiology* 2007;242:600–09

33. Nael K, Ruehm SG, Michaely HJ, et al. **High spatial-resolution CE-MRA of the carotid circulation with parallel imaging: comparison of image quality between 2 different acceleration factors at 3.0 Tesla.** *Invest Radiol* 2006;41:391–99